



system's behavior in the simplest and most concise way possible while still capturing its essential features. The method begins with the general dynamical systems form:

$$\frac{d\mathbf{x}(t)}{dt} = \mathbf{F}(\mathbf{x}(t)) \quad (1)$$

The function  $\mathbf{F}(\mathbf{x}(t))$  represents the dynamic constraints that specify the equations of motion of the system, and the vector  $\mathbf{x}(t)$  indicates the state of a system at time  $t$ .

In order to compute the function  $F$  from data, a time series of system's state variables  $\mathbf{x}(t)$  is collected. Also, the derivatives of state variables  $\dot{\mathbf{x}}(t)$  are measured or approximated numerically from  $\mathbf{x}(t)$  and arranged in the following matrix:

$$\dot{\mathbf{X}} = \begin{bmatrix} \dot{\mathbf{x}}^T(t_1) \\ \dot{\mathbf{x}}^T(t_2) \\ \vdots \\ \dot{\mathbf{x}}^T(t_T) \end{bmatrix} = \begin{bmatrix} \dot{x}_1(t_1) & \dot{x}_2(t_1) & \cdots & \dot{x}_K(t_1) \\ \dot{x}_1(t_2) & \dot{x}_2(t_2) & \cdots & \dot{x}_K(t_2) \\ \vdots & \vdots & \ddots & \vdots \\ \dot{x}_1(t_T) & \dot{x}_2(t_T) & \cdots & \dot{x}_K(t_T) \end{bmatrix} \quad (2)$$

Afterwards, a library  $\Theta(\mathbf{X})$  consisting of candidate nonlinear functions of the columns of  $\mathbf{X}$  is constructed. For instance,  $\Theta(\mathbf{X})$  may consist of constant, polynomial, and trigonometric terms:

$$\Theta(\mathbf{X}) = \begin{bmatrix} | & | & | & | & \cdots & | & | & | \\ 1 & \mathbf{X} & \mathbf{X}^{P_2} & \mathbf{X}^{P_3} & \cdots & \sin(\mathbf{X}) & \cos(\mathbf{X}) & \cdots \\ | & | & | & | & \cdots & | & | & | \end{bmatrix} \quad (3)$$

where, higher polynomials are shown as  $\mathbf{X}^{P_2}, \mathbf{X}^{P_3}, \dots$ . For example,  $\mathbf{X}^{P_2}$  denotes the quadratic nonlinearities in the state  $\mathbf{x}$ . A potential function for the right-hand side of Eq 1 is represented by each column of  $\Theta(\mathbf{X})$  in Eq 3. The values of each column are often normalized to prevent numerical instability and ensure that features contribute equally to the model fitting process. Since only a small number of these terms are active in each row of  $F$ , a sparse regression problem will be established to find the sparse vectors of coefficients  $\Xi = [\xi_1 \quad \xi_2 \quad \cdots \quad \xi_K]$  that determine which nonlinear terms are active:

$$\dot{\mathbf{X}} = \Theta(\mathbf{X})\Xi \quad (4)$$

For each column  $\xi_k$  of  $\Xi$ , there is a sparse vector of coefficients that determine which terms are active in the righthand side for one of the row equations  $\dot{\mathbf{x}}_k = \mathbf{F}_k(\mathbf{x})$  in Eq 1. After  $\Xi$  is identified, a model of each row of the governing equations can be built as follows:

$$\dot{\mathbf{x}}_k = \mathbf{F}_k(\mathbf{x}) = \Theta(\mathbf{x}^T)\xi_k \quad (5)$$

Unlike  $\Theta(\mathbf{X})$ , which is a data matrix,  $\Theta(\mathbf{x}^T)$  is a vector of symbolic functions of elements of  $\mathbf{x}$ . As a result,

$$\dot{\mathbf{x}} = \mathbf{F}(\mathbf{x}) = \Xi^T (\Theta(\mathbf{x}^T))^T \quad (6)$$

To obtain the sparse vector of coefficients  $\xi_k$  for the  $k$ th row equation, each column of  $\dot{\mathbf{X}}$  in Eq 4 requires a distinct optimization. Furthermore, the optimization is given by

$$\min_{\Xi} \frac{1}{2} \|\dot{\mathbf{X}} - \Theta(\mathbf{X})\Xi\|^2 + \lambda R(\Xi) \quad (7)$$

where  $\lambda$  is a hyper-parameter that controls the regularization's strength and  $R(\cdot)$  is a regularizer that encourages sparsity. There are several well-known techniques for Eq 7 when  $R(\cdot)$  is convex. The typical technique is to use  $R(\cdot)$  to represent the sparsity-promoting  $L1$  norm, which is a convex relaxation of the  $L0$  norm. While LASSO [17] is commonly used to solve SINDy due to its convex formulation, it has several limitations such as bias in coefficient estimation. Hence, the SINDy algorithm employs sequential thresholded least squares (STLSQ), which given a parameter  $\eta$  that specifies the minimum magnitude for a coefficient in  $\Xi$ , performs a least squares fit and then zeros out all the coefficients with magnitude below the threshold. This process of fitting and thresholding is repeated until convergence. The SINDy algorithm has recently been integrated into a python package PySINDy [18].

## 2.2 Graph Structured Time Series Data

Graphs provide a natural framework for representing systems where nodes (representing entities or states) and edges (representing interactions or connections) capture the underlying structure and dynamics of the network. The dynamics within a graph-structured system are governed by how changes in one node influence other nodes through their connections. This influence can be due to various factors such as physical interactions, information flow, or dependency relations. For instance, in a network of oscillators, the state of each oscillator at any given time is influenced by the states of the oscillators it is connected to, forming a complex web of interactions that evolve over time.

We represent the connections in the graph using an adjacency matrix  $A$ , where each element  $A_{ij}$  denotes the presence of a connection from node  $i$  to node  $j$ . In a directed graph,  $A_{ij}$  can differ from  $A_{ji}$ , indicating that the influence from node  $i$  to node  $j$  is not necessarily reciprocal. Connections in the graph, represented by the edges, signify the pathways through which information or influence is transmitted between nodes. These connections can be weighted to represent the varying strengths of interactions. For example, in a neural network, a stronger synaptic connection might result in a more significant influence of one neuron's activity on another.

## 3 MATERIALS AND METHOD

### 3.1 Method

The SINDyG method is based on SINDy algorithm which is described in Section 2. In SINDyG, shown in figure 1, the time history of the state variables  $\mathbf{X}$  are measured, their derivatives are calculated, and the structure of the network identified. Next, a library of functions of the states,  $\Theta(\mathbf{X})$ , is constructed. This feature library is used to find the fewest terms needed to satisfy  $\dot{\mathbf{X}} = \Theta(\mathbf{X})\Xi$  while taking into account the network structure. The few entries in the vectors of  $\Xi$  are identified using sparse regression [7]. Here, we provide details of each step of the SINDyG method.

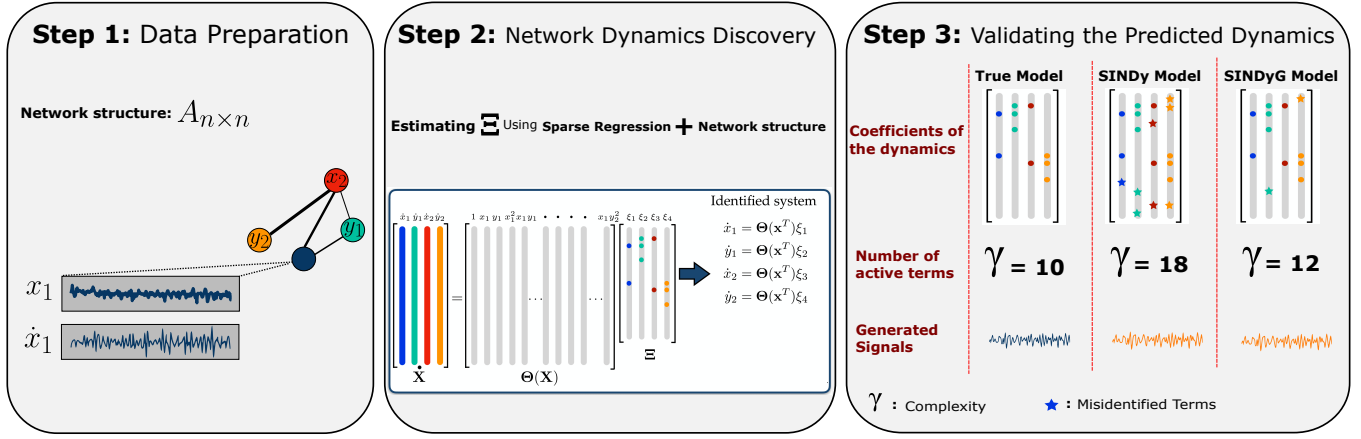


Fig. 1. Overview of the proposed framework for network dynamics discovery. Step 1: Data preparation involves collecting time-series data  $\mathbf{X}$  from a graph-structured system. Step 2: The SINDyG algorithm constructs a library of basis functions  $\Theta(\mathbf{X})$  and employs sparse regression to identify the optimal sparse coefficient matrix  $\Xi$  that satisfies  $\dot{\mathbf{X}} = \Theta(\mathbf{X})\Xi$ , while taking into account the network structure during the process. Step 3: The predicted dynamics are validated using appropriate metrics to assess model performance [7] [19].

### 3.1.1 Data Preparation

Data preparation is a crucial step in the discovery of dynamical systems using SINDyG method. This preparation involves gathering and organizing three key components: an adjacency matrix, time series data, and their derivatives. These components collectively provide the necessary information to uncover the underlying equations governing the system's behavior.

### 3.1.2 Network Dynamics Discovery

In this step, we aim to uncover the underlying dynamical equations governing each node in the network. We begin by constructing a library matrix,  $\Theta(\mathbf{X})$ , using a predefined set of basis functions. These basis functions represent potential terms that could contribute to the dynamics [7]. Next, we employ a sequentially thresholded least squares algorithm (STLSQ) [7] to determine the coefficients  $\Xi$  corresponding to these basis functions. This is achieved by minimizing the following objective function:

$$\min_{\Xi} \frac{1}{2} \|\dot{\mathbf{X}} - \Theta(\mathbf{X})\Xi\|_2^2 + \lambda \|f \cdot \Xi\|_2^2 \quad (8)$$

The parameter  $\lambda$  controls the sparsity of the solution, while the function  $f$  leverages the network's adjacency matrix ( $A$ ) to introduce a graph-aware penalty. This penalty term favors coefficients associated with strongly connected nodes and discourages those associated with weakly connected nodes, guiding the algorithm towards solutions that align with the network's structure. The intuition behind function  $f$  is to determine the relative importance of different terms in the library based on the network's connectivity. By establishing a mathematical relationship between the adjacency matrix and the desired active terms, we ensure that the discovered dynamics are consistent with the underlying network topology.

In order to calculate this penalty, we iterate through each candidate term,  $j$ , in the library of functions. For each term, we identify the source indices,  $S_j$ , representing the state variables present in term  $j$ . We then determine the sink

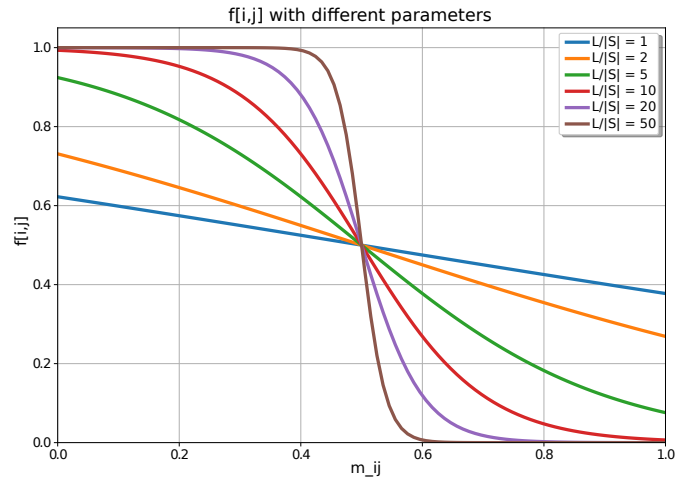


Fig. 2. Comparison of  $f[i, j]$  with different values of  $L/|S_j|$

indices,  $D_j$ , which are the state variables reachable from  $S_j$ . For each sink index  $i \in D_j$ , we compute the mean connectivity,  $m_{ij}$ , between the source group(s) and sink  $i$  using the adjacency matrix  $A$ . The penalty is then calculated using a function similar to the sigmoid function:

$$f[i, j] = \frac{1}{1 + \exp((L/|S_j|) \cdot (m_{ij} - 0.5))} \quad (9)$$

where  $L$  is a parameter for adjusting the shape of this function. As we increase  $L$ , the function becomes more similar to a step function. Conversely, if we reduce  $L$ , the function's behavior resembles a ramp function. This formulation ensures that terms with low mean connectivity between source and sink variables receive a higher penalty (closer to 1), while the penalty is scaled by the number of source variables,  $|S_j|$ , to account for terms involving multiple state variables. The shape of the function  $f[i, j]$  based on the value of  $L/|S_j|$  is illustrated in figure 2.

To solve the optimization problem shown in Eq. 8 for each state variable  $i$ , we perform a series of transformations

that allow us to leverage the standard ridge regression framework. First, we scale the feature matrix  $\Theta(X)$  and the coefficient vector  $\Xi_i$  to simplify the regularization term. Specifically, we define the transformed variables  $\Theta(X)'$  and  $\Xi_i'$  as follows:  $\Theta(X)' = \Theta(X) \cdot \text{diag}(1/f_i)$ , where each column  $j$  of  $\Theta(X)$  is divided by the corresponding element  $f_{ij}$ , and  $\Xi_i' = \text{diag}(f_i) \cdot \Xi_i$ , which scales each coefficient in  $\Xi_i$  by the corresponding element in  $f_i$ . These substitutions transform the original problem into the equivalent form  $\|\dot{X}_i - \Theta(X)'\Xi_i'\|_2^2 + \lambda\|\Xi_i'\|_2^2$ .

In this transformed space, the problem becomes a standard ridge regression, which can be solved efficiently using existing algorithms. After obtaining the solution  $\Xi_i'$  using sequentially thresholded least squares algorithm, we revert to the original coefficient vector  $\Xi_i$  by dividing  $\Xi_i'$  by  $f_i$ , ensuring that the final coefficients correspond to the original problem's scaling. This approach effectively incorporates the custom regularization term  $\lambda\|f_i \cdot \Xi_i\|_2^2$  into the ridge regression framework without altering the underlying algorithm. By scaling the feature matrix and coefficients appropriately, we maintain the efficiency of the standard ridge regression solver while addressing the modified regularization objective.

### 3.1.3 Validating the Predicted Dynamics

Once the underlying equations governing a system have been identified using techniques such as SINDy or SINDyG, a comprehensive validation process is essential to assess the model's performance. This involves evaluating the predicted model from multiple perspectives. Key metrics employed in this study include the model complexity index, Coefficient Error Index (CEI), generated signal accuracy, and training time.

The model complexity index ( $\gamma$ ) assesses the simplicity of the identified equations based on the number of active terms. A lower  $\gamma$  value signifies a more parsimonious model, potentially easier to interpret and generalizable. If the true mathematical equation describing the dynamics is known, the model complexity index could also be used to compare the complexity of the identified and true models allowing us to navigate the trade-off between accuracy and interpretability for more informative and reliable models. By considering model complexity with other metrics, we can ensure that the predicted model captures the essence of the system dynamics while remaining readily interpretable.

The Coefficient Error Index (CEI) evaluates the accuracy of the estimated coefficients, reflecting the model's fidelity to the underlying system. The CEI is calculated as the Mean Absolute Error (MAE) between the predicted coefficients and the true coefficients of the known dynamical model. Mathematically, the CEI is defined as:

$$\text{CEI} = \frac{1}{KC} \sum_{k=1}^K \sum_{c=1}^C \left| \xi_{k,c} - \hat{\xi}_{k,c} \right| \quad (10)$$

Here,  $K$  is the number of dynamical equations,  $C$  represents the number of different candidate functions for each equation,  $\xi_{k,c}$  denotes the  $c^{\text{th}}$  predicted coefficient for the  $k^{\text{th}}$  equation, and  $\hat{\xi}_{k,c}$  signifies the same thing but for true coefficient. A lower CEI value indicates a closer match

between the predicted and true coefficients, implying higher accuracy for the predicted dynamical model. Conversely, a higher CEI value suggests a larger discrepancy between the predicted and true values, signifying a potentially less accurate coefficient prediction. It should be noted that this method requires the availability of true coefficients. When the underlying governing equations are not readily available, alternative references such as values obtained from established physical laws or high-fidelity simulations could be employed.

The generated signal accuracy measure focuses on comparing the trajectories of state variables, specifically their derivatives, between the observed signal and the predicted signal. Two established metrics are employed for this comparison: R-squared ( $R^2$ ) and Mean Squared Error (MSE). The  $R^2$  quantifies the proportion of variance in the observed signal's derivatives explained by the predicted signal's derivatives by:

$$R^2 = 1 - \frac{\sum_{k=1}^K \sum_{i=1}^T \left( \hat{x}_k(t_i) - \bar{x}_k(t_i) \right)^2}{\sum_{k=1}^K \sum_{i=1}^T \left( \dot{x}_k(t_i) - \bar{\dot{x}}_k(t_i) \right)^2} \quad (11)$$

A higher  $R^2$  value indicates a stronger correlation between the two, suggesting the method effectively captures the dynamics governing the system. Conversely, a lower  $R^2$  value implies a weaker correlation, potentially indicating limitations in the method's ability to accurately predict the system's behavior.

Mean Squared Error (MSE) complements  $R^2$  by measuring the average squared difference between the observed and predicted signal's derivatives. A lower MSE signifies a closer match between the two, indicating higher accuracy in the predicted signal. Conversely, a higher MSE suggests a larger discrepancy, revealing potential shortcomings in replicating the observed or true system dynamics. MSE is defined as:

$$\text{MSE} = \frac{1}{KT} \sum_{k=1}^K \sum_{i=1}^T \left( \hat{x}_k(t_i) - \dot{x}_k(t_i) \right)^2 \quad (12)$$

Finally, the training time quantifies the computational efficiency of the model identification process. This is specially important for complex dynamical systems where the sparse regression models need to search through a vast library of candidate terms to discover the optimal sparse representation of the system dynamics.

## 4 EXPERIMENTS AND ANALYSIS

In this section, we will first introduce the different types of synthetic data used in this study and then compare the results of our proposed method with conventional SINDy approach.

### 4.1 Dataset

We have used a neuronal dynamics model to test and validate our proposed SINDyG method. At the neural level, the synchronized activity of large number of neurons can give rise to macroscopic oscillations [20]. These oscillations are an essential aspect of brain function, reflecting coordinated

neuronal activity that can be modeled in various ways [21]. One effective approach to model this oscillatory activity is using the Stuart-Landau (SL) equation [22]. The SL equation describes the behavior of a nonlinear oscillating system and could be used to model the internal dynamics of a group of neurons, capturing the essence of their collective behavior [22].

The SL equation in our study is defined as:

$$\dot{z} = (\sigma + i\omega - |z|^2) z \quad (13)$$

where  $z$  is a complex state representing the neuron's activity,  $\sigma$  is the parameter that dictates the growth rate of the oscillations, and  $\omega$  is the parameter that determines the oscillation frequency. For  $\sigma > 0$ , the model exhibits sustained oscillatory behavior with frequency  $\omega$ . This formulation captures the fundamental dynamics of neuronal oscillations within a population. To extend the SL equation for modeling interactions between neural populations, coupling dynamics is introduced. The extended model incorporates the effects of other neural populations or external inputs, represented by:

$$\dot{z}_n = (\sigma + i\omega - |z_n|^2) z_n + k z_n z_m \quad (14)$$

In this equation,  $z_n$  denotes the state of the  $n^{th}$  neuron, and  $z_m$  represents the dynamics of another interacting neural population. The coupling term  $k z_n z_m$  captures the influence of the  $m^{th}$  population on the  $n^{th}$  neuron's activity. This interaction term allows the model to account for the complex dynamics resulting from neural interactions. Each node's dynamics can be illustrated by a complex state,  $z = x + iy$ , which inherently represents a two-dimensional system due to its real and imaginary components ( $x$  and  $y$ ). By separating the real and imaginary components, we can decompose the complex dynamics into two independent equations, one governing the evolution of  $x$  and the other for  $y$ . This transformation allows us to analyze the system using familiar real-valued equations, effectively eliminating the need to directly work with complex quantities. By using this extended SL model, we can simulate the neural population dynamics under various conditions. Starting from an initial condition, we can calculate how the system evolves over time. This approach enables the generation of synthetic data that reflects the true dynamics of neuronal oscillations, which could be used to test our proposed method. We have considered a simple and more general case to validate our method.

#### 4.1.1 Simple Oscillatory Activity

In this section, the testing data is generated using the described SL oscillator framework in 14 for a simple case of graph-structured time series. In this case, as shown in figure 3, there are three interconnected nodes, each representing the dynamics of a group of neurons. Two of the nodes are connected, and one of them is isolated from the others. These nodes generate oscillatory behavior when starting from an initial condition. This oscillatory behavior is modeled by the SL equation and can be decomposed into its real and imaginary parts. the connectivity matrix of this

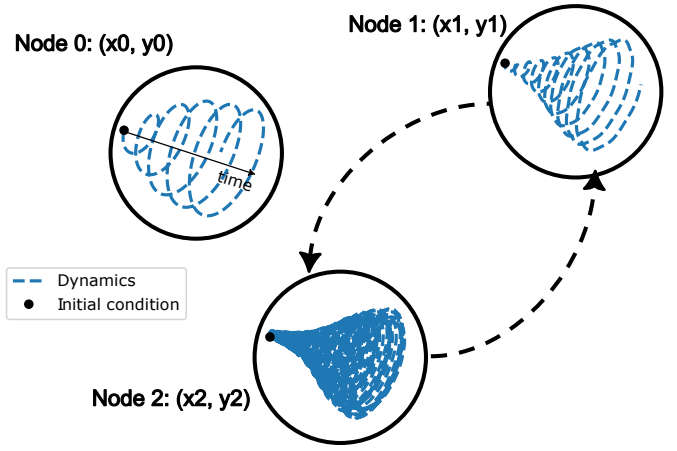


Fig. 3. Example of generated neuronal dynamics data to test SINDyG. The data is based on a simple network with three nodes where nodes 1 and 2 are connected. The parameters of the SL equation for this model include:  $\alpha = 0.2$  for all nodes, and  $\omega = \{\pi/2, \pi, 8\pi\}$ , for nodes 0, 1, and 2.

simple case is  $A = \begin{bmatrix} 0 & 0 & 0 \\ 0 & 0 & 1 \\ 0 & 1 & 0 \end{bmatrix}$ .

#### 4.1.2 General Oscillatory Activity

In this section, the dataset is generated in a flexible format to accommodate varying network sizes and structures. The number of nodes within the network is variable, and the connections between nodes adhere to the rules of either Erdős-Rényi (ER) [23] or scale-free (SF) [24] graph models. ER graphs feature randomly distributed edges, while SF networks exhibit a few highly connected hubs and a larger number of less connected nodes.

After the random generation of the graph structure, a coupling coefficient is assigned to each available edge. This coefficient represents the strength of the connection between nodes and quantifies how much the dynamics of one node influence another. Additionally, random parameters are chosen to govern the internal dynamics of each individual node. This approach allows for the exploration of a wide range of network configurations and dynamical behaviors within the dataset.

## 4.2 Results and Analysis

### 4.2.1 Simple Case Results

In this section, we delve into the results obtained from the simple case graph introduced earlier. This graph consists of three interconnected nodes, each governed by a specific dynamic. The true underlying model that generated the training data is known and visualized in figure 4. The heatmap columns represent the coefficients for each state variable's first-order differential equation, with higher values indicating stronger contributions from specific candidate terms. For instance, the first column reveals that only four candidate terms are active in the true model for that state variable.

In order to test our proposed model, we generated training data using the true dynamics in simple case study. This

training data comprises a single trajectory, starting from an initial point and capturing the system’s state evolution over a 20-second interval. This data was then used to train both SINDy and SINDyG models to uncover the underlying equations governing the system’s dynamics. For this training data, the SINDyG model achieved an R-squared score of 0.99999927 and an MSE of 0.00001297, outperforming the SINDy model which yielded an  $r^2$  score of 0.99999572 and an MSE of 0.00001352. Furthermore, we observed a slight advantage in computational efficiency for SINDyG. The time required for discovering the underlying equation using SINDyG was 0.04615 seconds, compared to 0.04858 seconds for SINDy.

Figure 4 presents a side-by-side comparison of the coefficients from the true model, the SINDy-predicted model, and the SINDyG-predicted model. The number of colored elements in each heatmap indicates the complexity of the model, with more active terms leading to higher complexity. A visual inspection reveals that the SINDy-predicted model has a higher number of active terms compared to the true model, resulting in greater complexity ( $\gamma = 62$ ). In contrast, the SINDyG-predicted model closely resembles the true dynamics and is more sparse compared to the SINDy-predicted model and the complexity for both the true and SINDyG-predicted model is  $\gamma = 32$ . We further quantify this similarity using the CEI (Coefficient Error Index), which measures the difference between the predicted and true coefficients. In this case, the SINDyG-predicted model achieves a low CEI score of 0.0033 outperforming the SINDy-predicted model’s CEI of 0.0155.

To further validate our models, we generated new trajectories by simulating the system from random initial conditions. These trajectories were not used in the discovery process and served as unseen test data. Figure 5 compares these generated signals with the trajectories produced using the true model. For a randomly generated new trajectory, the SINDyG model achieved  $r^2$  score of 0.99999935 and MSE of 0.00001736, outperforming the SINDy model which yielded an  $r^2$  score of 0.99988687 and MSE of 0.00009717. The R-squared score and Mean Squared Error (MSE) demonstrate that the model predicted by SINDyG outperforms the SINDy-predicted model. The results are also evident in figure 5, where the signals generated by the SINDyG-predicted model closely match those of the true model.

#### 4.2.2 General Case Results

In the general case, the network size, connectivity, and dynamics are variable and randomly chosen. We used the data from general case to conduct sensitivity analysis and assess the robustness of SINDy and SINDyG methods. Figure 6 presents the results for various performance metrics, including complexity, CEI, training time, training  $r^2$  and MSE, as well as testing  $r^2$  and MSE scores.

The first column of figure 6 examines the impact of increasing the number of oscillators in the network. As the network size grows, so does the number of connections and the complexity of the dynamical equations for each node. This leads to an expected increase in complexity for both methods. However, SINDyG consistently yields

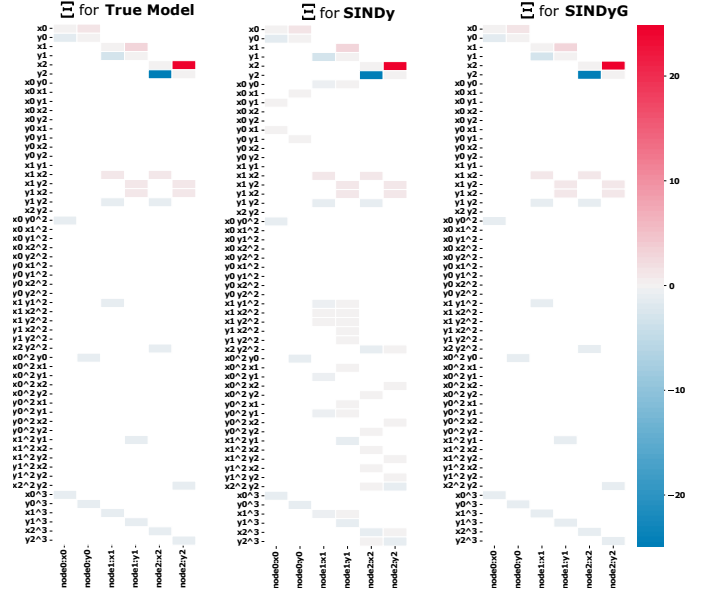


Fig. 4. The heatmap showing the coefficients of extracted dynamical models using SINDy and SINDyG. The SINDyG extracted a much simpler model ( $\gamma = 32$ ), when compared to the SINDy with  $\gamma = 62$ .

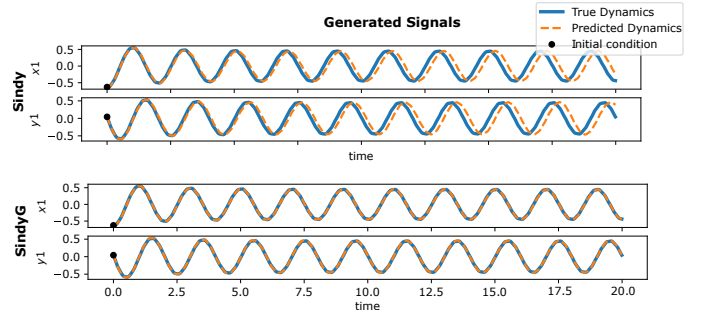


Fig. 5. True and predicted trajectories of node 1 in simple case study from the same initial condition for SINDy and SINDyG. The  $r^2$  score for SINDyG was 0.9999997, which is higher than the  $r^2$  score of 0.9997024 for SINDy.

models with lower complexity, regardless of the network size. Additionally, the CEI decreases as the number of nodes increases, which is in line with the characteristics of CEI for larger sets of potential coefficients. Importantly, SINDyG consistently outperforms SINDy in terms of CEI, indicating closer alignment with the true coefficients. While the training time remains relatively consistent for both methods, the train R-squared and MSE worsen for SINDy as the number of nodes increases, whereas SINDyG maintains performance. This trend extends to the test MSE and R-squared, highlighting SINDyG’s ability to generalize to new, unseen data, especially in larger networks.

The second column explores the effect of increasing the maximum allowed value for edge weights, resulting in larger coupling term coefficients in the discovered equations. SINDy’s complexity increases dramatically with higher edge values, while SINDyG exhibits only a marginal increase. This discrepancy also leads to a substantial rise in CEI for the SINDy-predicted model, indicating a significant



deviation from the true coefficients. Furthermore, the training time for both methods noticeably increases as the coefficient values rise. In the third column, we vary the value of the hyperparameter ( $L$ ) in the penalty function ( $f[i, j]$ ). As  $L$  increases, the results become more robust, leading to enhanced predictive power for both methods. The fourth column focuses on the impact of varying the training length, effectively reducing the amount of training data available. We observe that SINDy's performance deteriorates as the data size gets smaller. In both predicted models, when we increase the train data the results are more robust as the standard error decreases.

Overall, SINDy struggles with larger graphs and high coupling values, and its predictive power diminishes with limited training data. In contrast, SINDyG demonstrates greater resilience and consistently superior performance across various scenarios. Furthermore, SINDyG demonstrates more robust performance given significantly smaller standard errors compared to SINDy. This is also evident by the summary results provided in Table 1.

## 5 CONCLUSION

The main contribution of this study is the development of a novel method called SINDyG, which integrates network structure into sparse regression for the identification of governing equations in graph-structured dynamical systems. By incorporating the network structure, SINDyG not only improves the accuracy of the identified models but also simplifies them, making the results more interpretable. These models can be generalized to unseen data, demonstrating the robustness of SINDyG in capturing the essential dynamics of complex systems. Our proposed method opens new avenues for understanding and predicting the behavior of complex systems in various fields, including neuroscience, ecology, finance, and epidemiology.

The primary limitation of the proposed method is the selection of appropriate basis or library functions, which could be challenging for complex systems with stochastic behavior. The size of the library function also impacts the computational complexity, which could be managed using regularization parameters. Lastly, while the method's performance was validated with synthetic data, further research is needed to assess its effectiveness on real-world datasets where the true underlying dynamics are unknown.

Building on the insights from our study, future efforts could be dedicated to improving the inference of stochastic system dynamics by investigating alternative stochastic models that more accurately capture the inherent variability found in empirical systems. Additionally, deep learning models such as reinforcement learning could improve the inference capabilities for complex system dynamics, particularly when dealing with incomplete real-world data that has unobserved nodes and missing links.

## 6 CODE AND DATA AVAILABILITY

All the code and data used in this study are available at: <https://github.com/3sigmalab/SINDyG>

## REFERENCES

- [1] V. Marx, "The big challenges of big data," *Nature*, vol. 498, no. 7453, pp. 255–260, 2013.
- [2] J. Bongard and H. Lipson, "Automated reverse engineering of nonlinear dynamical systems," *Proceedings of the National Academy of Sciences*, vol. 104, no. 24, pp. 9943–9948, 2007.
- [3] M. Schmidt and H. Lipson, "Distilling free-form natural laws from experimental data," *science*, vol. 324, no. 5923, pp. 81–85, 2009.
- [4] J. Koza, "On the programming of computers by means of natural selection," *Genetic programming*, 1992.
- [5] I. G. Kevrekidis, C. W. Gear, J. M. Hyman, P. G. Kevrekidis, O. Runborg, C. Theodoropoulos *et al.*, "Equation-free, coarse-grained multiscale computation: enabling microscopic simulators to perform system-level analysis," *Commun. Math. Sci*, vol. 1, no. 4, pp. 715–762, 2003.
- [6] G. Sugihara, R. May, H. Ye, C.-h. Hsieh, E. Deyle, M. Fogarty, and S. Munch, "Detecting causality in complex ecosystems," *science*, vol. 338, no. 6106, pp. 496–500, 2012.
- [7] S. L. Brunton, J. L. Proctor, and J. N. Kutz, "Discovering governing equations from data by sparse identification of nonlinear dynamical systems," *Proceedings of the national academy of sciences*, vol. 113, no. 15, pp. 3932–3937, 2016.
- [8] J.-C. Loiseau and S. L. Brunton, "Constrained sparse galerkin regression," *Journal of Fluid Mechanics*, vol. 838, pp. 42–67, 2018.
- [9] P. Zheng, T. Askham, S. L. Brunton, J. N. Kutz, and A. Y. Aravkin, "A unified framework for sparse relaxed regularized regression: Sr3," *IEEE Access*, vol. 7, pp. 1404–1423, 2018.
- [10] R. Li, C. Sun, M. Dong, M. Wang, Q. Gao, and X. Liu, "The controllability analysis of brain networks during rhythmic propagation," *IEEE Transactions on Network Science and Engineering*, vol. 11, no. 4, pp. 3812–3823, 2024.
- [11] U. Nakarmi, M. Rahnamay-Naeini, and H. Khamfroush, "Critical component analysis in cascading failures for power grids using community structures in interaction graphs," *IEEE Transactions on Network Science and Engineering*, vol. 7, no. 3, pp. 1079–1093, 2019.
- [12] J. Becker, D. Brackbill, and D. Centola, "Network dynamics of social influence in the wisdom of crowds," *Proceedings of the national academy of sciences*, vol. 114, no. 26, pp. E5070–E5076, 2017.
- [13] Q. Zhang, K. Yu, Z. Guo, S. Garg, J. J. P. C. Rodrigues, M. M. Hassan, and M. Guizani, "Graph neural network-driven traffic forecasting for the connected internet of vehicles," *IEEE Transactions on Network Science and Engineering*, vol. 9, no. 5, pp. 3015–3027, 2022.
- [14] S. H. Strogatz, "Exploring complex networks," *nature*, vol. 410, no. 6825, pp. 268–276, 2001.
- [15] T.-T. Gao and G. Yan, "Autonomous inference of complex network dynamics from incomplete and noisy data," *Nature Computational Science*, vol. 2, no. 3, pp. 160–168, 2022.
- [16] F. Battiston, G. Cencetti, I. Iacopini, V. Latora, M. Lucas, A. Patania, J.-G. Young, and G. Petri, "Networks beyond pairwise interactions: Structure and dynamics," *Physics reports*, vol. 874, pp. 1–92, 2020.
- [17] T. Hastie, R. Tibshirani, and M. Wainwright, *Statistical learning with sparsity: the lasso and generalizations*. CRC press, 2015.
- [18] B. M. de Silva, K. Champion, M. Quade, J.-C. Loiseau, J. N. Kutz, and S. L. Brunton, "Pysindy: a python package for the sparse identification of nonlinear dynamics from data," *arXiv preprint arXiv:2004.08424*, 2020.
- [19] K. Champion, S. L. Brunton, and J. N. Kutz, "Discovery of nonlinear multiscale systems: Sampling strategies and embeddings," *arXiv preprint arXiv:1805.07411*, 2018.
- [20] N. J. Napoli, M. Demas, C. L. Stephens, K. D. Kennedy, A. R. Harrivel, L. E. Barnes, and A. T. Pope, "Activation complexity: A cognitive impairment tool for characterizing neuro-isolation," *Scientific Reports*, vol. 10, no. 1, p. 3909, 2020.
- [21] K. B. Doelling and M. F. Assaneo, "Neural oscillations are a start toward understanding brain activity rather than the end," *PLoS biology*, vol. 19, no. 5, p. e3001234, 2021.
- [22] Y. Qin, T. Menara, D. S. Bassett, and F. Pasqualetti, "Phase-amplitude coupling in neuronal oscillator networks," *Physical Review Research*, vol. 3, no. 2, p. 023218, 2021.
- [23] P. Erdos, A. Rényi *et al.*, "On the evolution of random graphs," *Publ. math. inst. hung. acad. sci.*, vol. 5, no. 1, pp. 17–60, 1960.
- [24] K.-I. Goh, B. Kahng, and D. Kim, "Universal behavior of load distribution in scale-free networks," *Physical review letters*, vol. 87, no. 27, p. 278701, 2001.

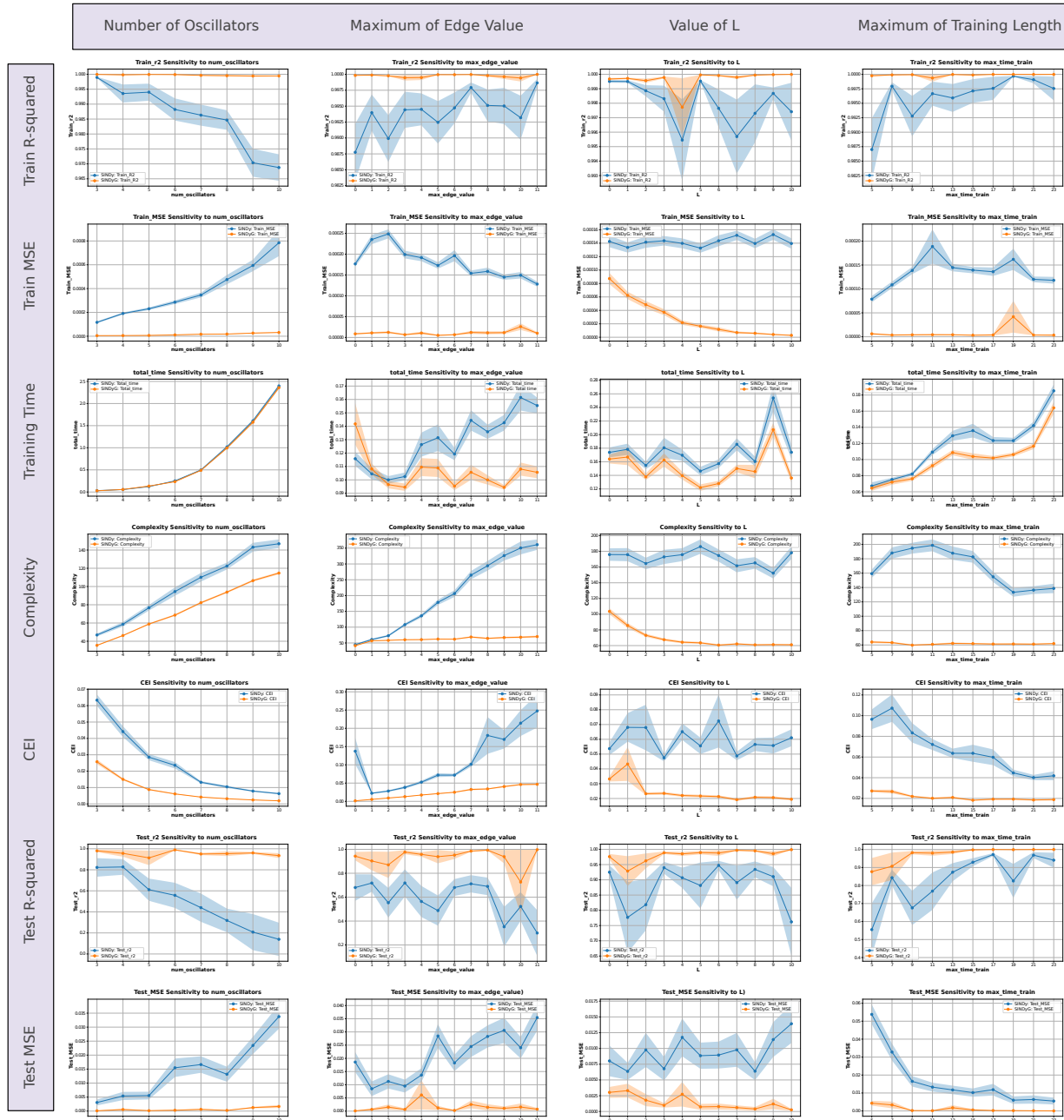


Fig. 6. Sensitivity analysis of different parameters in the general case. The results are based on 100 repetitions and show the mean and standard error for different performance metrics.



**Mohammad Amin Basiri** is a PhD candidate in the Data Science and Analytics program at the University of Oklahoma. He holds a Master's degree from the University of Tehran and a Bachelor's degree from Amirkabir University, both in Electrical Engineering with a focus on machine learning and artificial intelligence. His research focuses on developing advanced, data-driven techniques to model and understand complex systems.



**Sina Khanmohammadi** Dr. Sina Khanmohammadi is an assistant professor in the School of Computer Science at the University of Oklahoma. Prior to joining OU, he was a Postdoctoral Associate in the Department of Electrical & Systems Engineering at Washington University in St. Louis. Dr. Khanmohammadi has received his Ph.D. in Systems Science from the State University of New York at Binghamton, M.Sc. in Manufacturing Management from the University of Hertfordshire in UK, and B.Sc. in Computer Science from the University of Tabriz in Iran. His research involves using neuroimaging datasets to understand the underlying principles and mechanism that govern cognitive functions and how they get disrupted due to various brain-related disorders.



TABLE 1  
Performance Metrics of SINDy and SINDyG on 100 Different Graphs with 5 Oscillators based on Graph Types (Mean  $\pm$  SE)

Metric	ER		SF	
	SINDy	SINDyG	SINDy	SINDyG
Complexity	76.470 $\pm$ 3.4615	61.870 $\pm$ 0.8531	71.790 $\pm$ 2.9351	59.410 $\pm$ 0.7261
CEI	0.0323 $\pm$ 0.0026	0.0107 $\pm$ 0.0004	0.0267 $\pm$ 0.0015	0.0086 $\pm$ 0.0003
Train_time	0.1224 $\pm$ 0.0059	0.1244 $\pm$ 0.0049	0.1408 $\pm$ 0.0111	0.1393 $\pm$ 0.0096
Train_r2	0.9937 $\pm$ 0.0029	0.9993 $\pm$ 0.0005	0.9884 $\pm$ 0.0041	0.9998 $\pm$ 0.0001
Train_MSE	0.0003 $\pm$ 0.0000	0.0000 $\pm$ 0.0000	0.0002 $\pm$ 0.0000	0.0000 $\pm$ 0.0000
Test_r2	0.5861 $\pm$ 0.1143	0.9732 $\pm$ 0.0126	0.5973 $\pm$ 0.1257	0.9715 $\pm$ 0.0127
Test_MSE	0.0076 $\pm$ 0.0017	0.0003 $\pm$ 0.0001	0.0067 $\pm$ 0.0013	0.0013 $\pm$ 0.0012